DOI: 10.21062/mft.2026.004 http://www.journalmt.com

Effect of Machining on 3D Surface Texture and Scratch Resistance of Structural Steel

Eva Jurickova (0000-0002-8018-7391)[1], Oskar Zemcik (0000-0001-7786-3531)[2], Stepan Kolomy (0000-0003-3781-692X)[2], Josef Sedlak (0000-0002-9819-8259)[1], Denisa Hrusecka (0000-0003-1459-0040)[1], Felicita Chromjakova (0000-0002-5084-1153)[1], Petra Sliwkova (0000-0003-4121-2168)[2]
[1]Tomas Bata University in Zlín, Faculty of Management and Economics, Department of Industrial Engineering and Information Systems, Mostní 5139, Zlín 760 01, Czech Republic
[2]Institute of Manufacturing Technology, Faculty of Mechanical Engineering, Brno University of Technology, Czech Republic

This study experimentally compares how three common machining routes, turning, milling and grinding, affect the surface texture and tribological response of three structural steels (C45, 42CrMo4, 30CrMoV9) under conditions where the profile roughness Ra is deliberately aligned across routes. Areal topography was measured by coherence correlation interferometry and evaluated according to ISO 21920-2 (height metrics Sa, Sq, Sp, Sv, Sz, St). The bearing area curve (Abbott–Firestone) was used to derive functional descriptors Rpk, Rk and Rvk. Scratch resistance was determined on a UMT-3 tribometer (Rockwell 120°, P = 50 N) as HSp = 8·P / w² in accordance with ASTM G171. The results show that surfaces with comparable Ra can differ markedly in areal extremes and BAC-derived parameters, which is reflected in scratch response. These findings support replacing sole Ra specification with areal and bearing-curve descriptors when functional performance is critical (friction, sealing, wear).

Keywords: Areal parameters, Bearing area curve (BAC), 3D surface texture, Scratch resistance, ASTM G171.

1 Introduction

Surface texture critically governs friction, the formation and stability of lubricating films, sealing capability, and wear mechanisms of engineering components. In industrial practice, quality acceptance has traditionally relied on 2D profile indicators, most notably the arithmetic mean roughness, Ra, which represents only a single line and thus reduce inherently areal information to a one-dimensional section. As a result, identical Ra values may correspond to topographies and functional behaviours that differ substantially in real tribological contact [1-3].

Over the past two decades, surface metrology has undergone a paradigm shift towards areal (3D) characterisation, codified by the ISO 21920-2 framework. Areal parameters, height (Sa, Sq, Sp, Sv, Sz), spatial (e.g., Sal, Str), hybrid, and functional, provide a planar description of topography, including extremes and the distribution of heights, with tighter links to function than purely profile indicators [4-5]. In parallel, the profile branch has been modernised through ISO 21920-2, which harmonises terminology and brings profile evaluation closer to the areal approach [6-7].

Functionally, areal extremes (Sz, St) are particularly important because they relate to damage initiation and local film overload, whereas the height-distribution shape (Ssk, Sku) and spatial descriptors of anisotropy and scale (Sal, Str) capture whether the surface forms a continuous load-bearing platform and provides valleys for lubricant retention - factors with a direct impact on friction and wear [1,3].

Complementary to this, analysis of the bearing area curve (Abbott–Firestone) has proved practical. From profile data, the Rk family (Rpk - reduced peak height; Rk - core depth; Rvk - reduced valley depth) yields a 'map of function': Rpk relates to film rupture during run-in, Rk to the load-bearing core, and Rvk to lubricant retention and debris accommodation. The areal standard ISO 21920-2 introduces the analogous Sk family (Spk, Sk, Svk, and material ratios), which refines the interpretation in 3D [3,6-7]. A judicious choice of these parameters markedly increases discrimination between machining routes and between surfaces sharing the same Ra but differing morphology [1-3, 8].

Different machining routes (turning, milling, grinding) produce distinct textures (periodicity, lay orientation, peak-to-valley balance). Even at comparable Ra, they may differ markedly in areal extremes and bearing-curve descriptors and thus in service behaviour [2, 9]. Tool condition (e.g., grinding-wheel wear and balance) further shifts extremes, lay and functional descriptors, underlining

the need to evaluate more than just average profile roughness.

Scratch tests are commonly used to probe resistance to mechanical damage. ASTM G171 defines a method to determine scratch 'hardness/resistance' from residual tracks under a defined indenter; a standard interpretation uses $HSp = kP/w^2$ ($k = 8$) relating normal load P to residual width w [8]. The scratch response is governed by both material properties (hardness, microstructure) and surface morphology (extremes, BAC/Sk family, anisotropy), precisely the features quantified by 3D metrology [1-3, 8].

Finally, functional topographies can be engineered deliberately: laser surface texturing (LST) creates micro-dimples that act as micro-bearings, lubricant reservoirs or debris traps, improving friction and wear, demonstrated in classic work by Etsion [9] and substantiated by more recent reviews [1]. This context further underscores why sole control of Ra is insufficient for functional surface specification.

Accordingly, this study examines whether and to what extent 3D areal parameters (especially extremes Sz, St) together with bearing-curve descriptors (Rpk, Rk, Rvk) explain differences in scratch response between machined steels when Ra is deliberately aligned across routes. This aligns with the community's transition from profile to areal metrology advocated by standards and reviews alike [1-3, 6-7]. The workflow is shown in Figure 1.

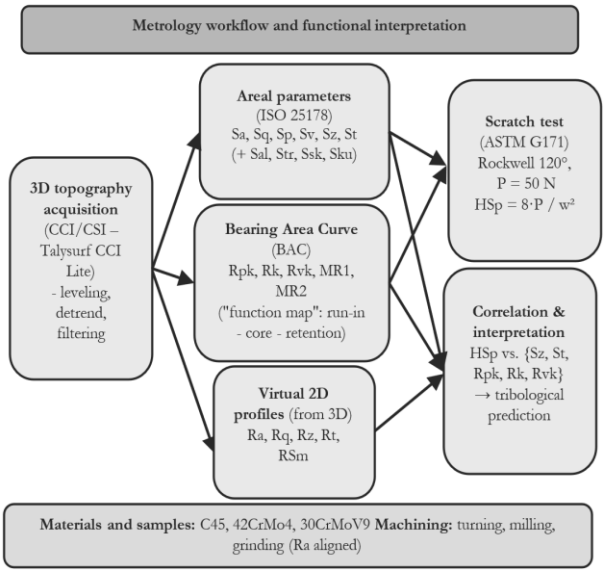

Fig. 1 *Metrology workflow and functional interpretation*

2 Materials and Methods

2.1 Materials and machining routes

Three engineering steels (the chemical compositions in given in Tab. 1) were investigated: C45 (ČSN 41 2050), 42CrMo4 (ČSN 41 5142) and 30CrMoV9 (ČSN 41 5330). All blanks were heat treated by quenching and tempering to obtain comparable baseline mechanical properties across alloys. The chemical composition of each batch was verified by spark OES (Bruker Q4 Tasman).

Tab. 1 *Chemical composition of the machined materials*

Wo (%)	C	Mn	Si	Cr	Mo	V	P	S
C45	0.42 – 0.50	0.50 – 0.80	0.17 – 0.37	max. 0.40	—	—	max. 0.045	max. 0.045
42CrMo4	0.38 – 0.45	0.60 – 0.90	0.17 – 0.37	0.90 – 1.20	0.15 – 0.30	—	max. 0.025	max. 0.035
30CrMoV9	0.26 – 0.34	0.40 – 0.70	max. 0.40	2.30 – 2.70	0.15 – 0.25	0.10 – 0.20	max. 0.025	max. 0.025

Specimens were then prepared by three machining routes: turning (CNC lathe Kovosvit MAS SP 280 SY) using the indexable cutting inserts made from sintered carbides. milling (TOS FV 252 CNC A) when applying endmill and grinding (TOS BPH 320 A) with the Al_2O_3 material. Cutting parameters (cutting speed. feed. depth of cut) were tuned per material and route with the explicit target to achieve mutually comparable profile roughness Ra across routes. so that functional differences reflect texture morphology rather than the average profile roughness. For grinding. the condition of the wheel (dressing. centring. wear/balance) was documented because it critically affects areal extremes and bearing-curve descriptors. Coolant regime and fixturing were kept consistent within each route. A consolidated overview of machines and process settings is provided in Table 2.

Tab. 2 *Machines and process conditions (routes tuned to comparable Ra). instruments and evaluation settings*

Turning machine - Kovosvit MAS SP 280SY
spindle speed n = 1040 min^{-1}; feed f = 0.10 mm; cutting speed v_c = 150 m.min^{-1}; ambient temperature t = 22 °C; nose radius r_ε = 1.2 mm.
Milling machine - TOS FV 25 CNC A (FV 252 CNC A)
spindle speed n = 955 min^{-1}; tooth feed fz = 0.05 mm.tooth^{-1}; cutting speed v_c = 150 m.min^{-1}; ambient temperature 22 °C.
Surface grinder - TOS BPH 320 A
infeed = 3.0 mm; tangential cutting feed = 12 m.min^{-1}; depth of cut ap = 0.01 mm; cutting speed v_c = 40 m.s^{-1}; ambient temperature 22 °C.
Spark OES spectrometer - Bruker Q4 Tasman
Fe-base low-alloy; P60–P120 grind + degrease; Ar ≥99.998% purge; pre-burn ~3 s; acquire 2–3 s; 4–5 burns (1st conditioning); CRM standardization/drift
Vickers hardness tester - LECO LV 800 AT
Settings used: Vickers HV10; load = 10 kgf; dwell = 10 s; ambient 22 °C.
3D optical profiler - Taylor Hobson Talysurf CCI Lite
measured area 0.8 × 0.8 mm; series of 1024 extracted profiles; base length 0.8 mm; Gaussian filter 0.25 mm (per ISO methods).
Tribometer (scratch) - Bruker UMT-3. Rockwell diamond 120°
Scratch test per ASTM G171: constant normal load P = 50 N; track length 10 mm; minimum spacing between scratches ≥ 5× track width. Wear-scar profiling with inductive probe (resolution 10 nm). scan step 3 µm; evaluated length 300 µm.

2.2 Surface metrology and data reduction

Surface topography was measured by coherence correlation interferometry (CCI/CSI) using a Taylor Hobson Talysurf CCI Lite. which offers high vertical resolution and low measurement noise suitable for engineered surfaces [3]. For each condition (steel × route). repeated areal maps were acquired at representative. defect-free locations. Acquisition settings (objective. lateral sampling pitch. evaluation area) and the pre-processing pipeline were kept identical across all measurements.

Pre-processing comprised plane levelling/form removal (least-squares) and a consistent noise-suppression step; no parameters were evaluated until the same pre-processing had been applied to all datasets [3]. Areal parameters were computed according to ISO 25178-2 height metrics Sa, Sq, Sp, Sv, Sz and St (optionally complemented by Sal, Str, Ssk and Sku) [6]. The bearing-area curve (Abbott–Firestone) was analysed to obtain Rpk, Rk and Rvk as functional descriptors of run-in peaks. core load-bearing depth and lubricant-retaining valleys. For comparability with industrial practice. 2D profile parameters Ra, Rq, Rz, Rt and RSm were extracted from the 3D maps as virtual profiles using a consistent sampling strategy; definitions follow ISO 21920-2 [7]. Reported values are means of repeated maps per specimen. and specimen-level results are summarised as mean ± SD per condition.

2.3 Scratch testing and hardness

Scratch response was measured on a Bruker UMT-3 tribometer using a Rockwell diamond cone (120°) under constant normal load P = 50 N in accordance with ASTM G171 [8]. Residual scratch width w was evaluated at predefined positions along the track (e.g.. 2/5/8 mm from the start); where applicable. residual depths and damaged areas were also recorded by profilometry. Scratch resistance was computed as $HSp = 8 \cdot P / w^2$. with P in newtons and w in metres. yielding a comparative hardness-like index sensitive to material strength and surface integrity [8]. For each specimen and condition. multiple parallel scratches were produced and summarised as mean ± SD.

Vickers hardness HV10 (LECO LV 800 AT) was measured on each specimen (≥3 indents per specimen with spacing ≥3× the diagonal). Hardness values are reported as specimen means and used to contextualise scratch results (material-dominated trend vs. secondary process effects). Results throughout the paper are presented descriptively as mean ± SD (and ranges where helpful); no inferential hypothesis tests were performed.

3 Results and Discussion

3.1 Profile vs areal: different sensitivity to process signatures

Despite tuning cutting conditions to achieve comparable line-based roughness Ra across all three machining routes and steels. the areal height extremes Sz and St separated the processes far more clearly. Figure 2 shows representative optical macrographs (≈1×1 mm FOV) for grinding. milling and turning. evidencing distinct texture anisotropy and defect populations. Figure 3 presents areal maps (Talysurf CCI Lite) at matched Ra. highlighting that turning suppresses tall peaks and deep dales relative to milling and. especially. grinding.

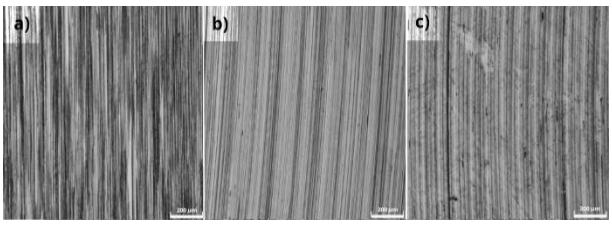

Fig. 2 *Representative optical macrographs (≈ 1×1 mm FOV) for (a) grinding, (b) milling, and (c) turning illustrate different texture anisotropy and defect populations. Acquisition: Olympus DSX 500*

Interpretation. Compared with profile descriptors. areal parameters integrate spatial variability and capture peak/dale outliers that dominate contact initiation. film rupture and debris trapping; as a result. they may re-rank processes relative to Ra-based judgements [1-3, 9, 10]. This is consistent with metrology guidance and industrial surveys recommending 3D parameters for functional specification [2, 3].

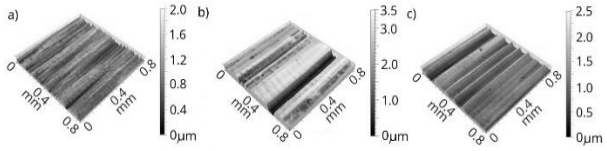

Fig. 3 *3D surface texture maps for (a) grinding, (b) milling and (c) turning*

3.2 Material ratio curve (BAC): functional trade-offs captured by the Rk family

Material-ratio-curve metrics exposed a mechanistic trade-off among run-in behaviour. core load capacity and lubricant retention: in our dataset. Rpk (reduced peak height) and Rk (core roughness) were generally lowest for turning. indicating fewer protruding summits and a more stable plateau; Rvk (reduced valley depth) tended to be highest for grinding. consistent with deeper lubricant-retaining valleys (albeit accompanied by larger extremes). Figure 4 compiles virtual profiles (extracted from the same 3D maps) across the tool-path direction for turning. milling and grinding. illustrating the differing peak/valley populations that drive BAC metrics [11-14].

The functional reading - peaks governing early wear and film rupture; valleys aiding transient reservoir effects is in line with prior analyses linking Spk/Rpk to run-in and Svk/Rvk to lubricant support [15-18]. The relatively poorer ground surfaces observed here are coherent with the strong influence of grinding wheel topography/conditioning on extremes and subsurface integrity [19-23]. Representative Abbott–Firestone curves for all three steels are shown in Figure 5.

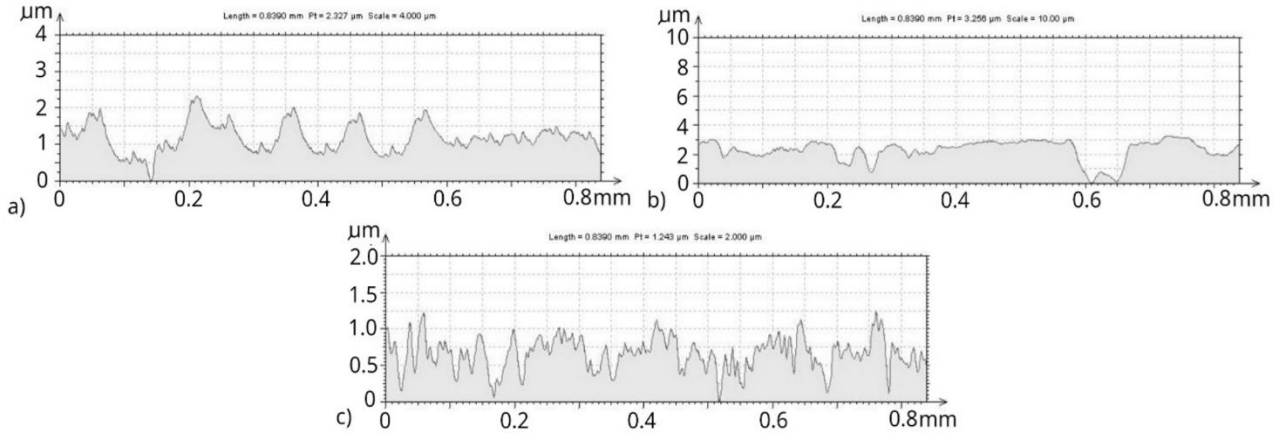

Fig. 4 *Surface profiles across the tool path for samples machined by (a) turning, (b) milling and (c) grinding*

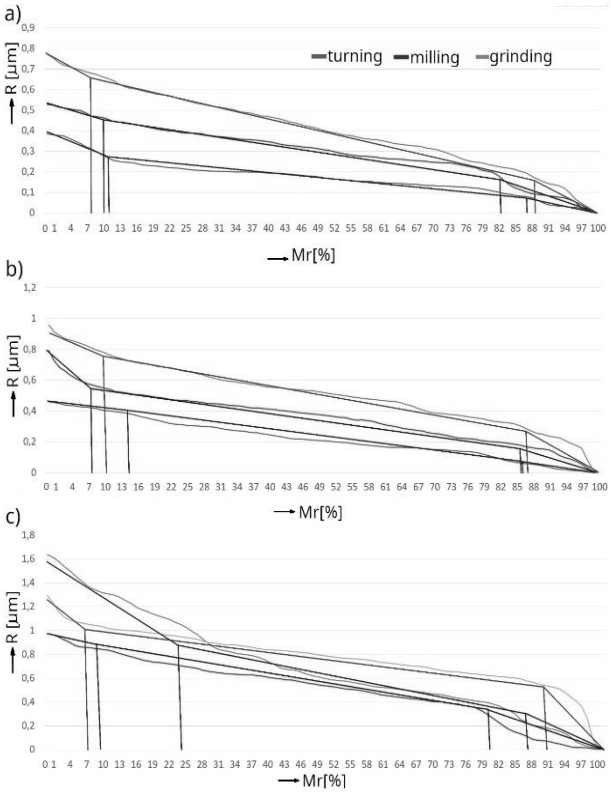

Fig. 5 *Abbott–Firestone curve with marked Mr1, Mr2, Rpk, Rk and Rvk limits a) C45 b) 42CrMo4 c) 30CrMoV9*

3.3 Scratch resistance and hardness

The scratch hardness number HSp (ASTM G171) scaled primarily with steel grade hardness (C45 < 42CrMo4 < 30CrMoV9 per HV10). as expected for plastically dominated scratching. A secondary. consistent process effect was also evident: turning delivered the highest HSp (narrower residual grooves). while grinding produced the lowest HSp (wider grooves). mirroring the Sz/St and Rpk trends.

Peak-dominated textures (high Spk/Rpk) concentrate local contact stresses and admit deeper scratches at identical load; plateaued textures with lower extremes distribute load and limit plastic ploughing [24, 25]. Consequently. combining areal extremes with BAC parameters adds predictive power beyond Ra alone for damage-tolerance ranking [26].

Figure 6 summarises HSp together with the residual groove metrics (Ar. hr) by process within each steel. A consistent ordering emerges: turning exhibits the highest HSp (and the smallest Ar/hr). milling is intermediate. and grinding the lowest HSp. The effect is modest for C45 and more pronounced for 42CrMo4 and 30CrMoV9. in line with the areal extremes and peak content discussed earlier. These co-trends corroborate the interpretation that peak/dale geometry. rather than Ra. governs damage tolerance under the present conditions [27].

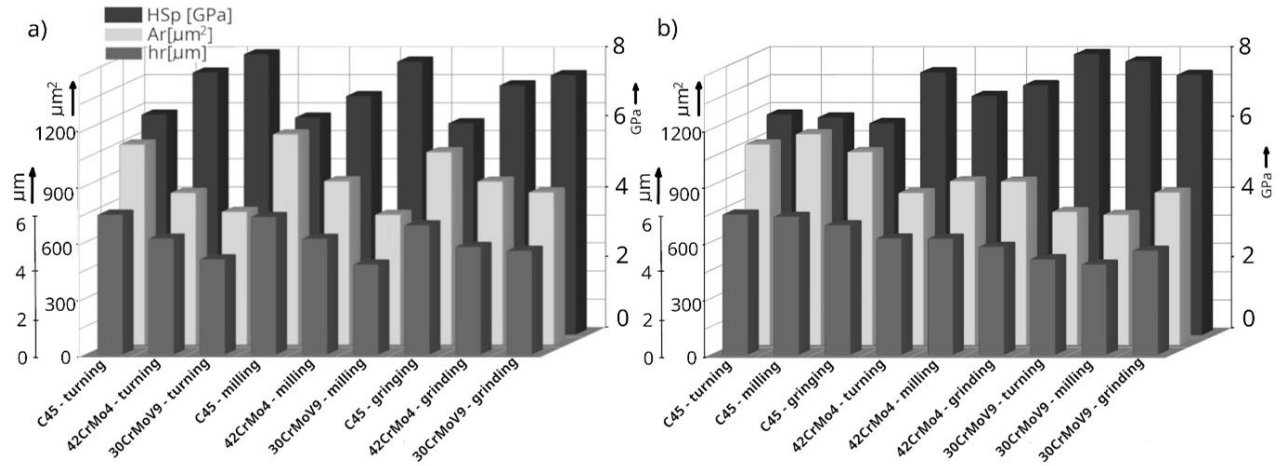

Fig. 6 *Scratch response by process within each steel. Bars show scratch hardness HSp (GPa). residual groove area Ar (µm²) and residual groove depth hr (µm) for C45. 42CrMo4 and 30CrMoV9 at constant load (ASTM G171). Values are means (≈ 3 replicates per route) a) ordered by machining type b) ordered by material*

3.4 Process-texture–function linkage (qualitative synthesis)

Across steels. the turning route delivered the lowest areal extremes and peak content (favourable for run-in stability and reduced film rupture). milling sat intermediate with occasional isolated defects. and grinding showed the largest extremes and the deepest valleys (potentially aiding lubricant retention but penalising peak-driven damage). This qualitative linkage-process texture signature tribological response aligns with broader studies correlating 3D parameters to friction/wear and with critiques of over-reliance on single-line Ra [28, 29].

3.5 Practical implications and limitations

For functional specifications. supplement (or replace) Ra with areal extremes (Sz, St) and bearing-area-curve (BAC) parameters (Rpk, Rk, Rvk). and always report relevant process context (e.g. grinding wheel state. dressing and balance) [30]. Where run-in

stability and lubricant-film integrity are critical. specify upper bounds on peak-dominated metrics (Spk/Rpk) and on extremes (Sz). For starved or mixed-lubrication duty. constrain valley descriptors (Svk/Rvk) together with extremes to avoid peak-induced scuffing [31].

Replication per variant was modest (approximately n = 3). and the wheel condition during grinding is a confounding covariate. The correlation analysis introduced here (Fig. 7) is exploratory given the small sample size; coefficients are shown without hypothesis testing or multiple-comparison control and should be interpreted descriptively. Some 3D functional parameters (e.g. Spk, Svk) were not available from the original evaluation. Future work should (i) expand n to enable confidence intervals/uncertainty. (ii) include directionality metrics (Str. Sal) and partial correlations controlling for hardness. and (iii) maintain strict ISO-compliant filtering (ISO 16610) with full traceability of processing steps [32-35]

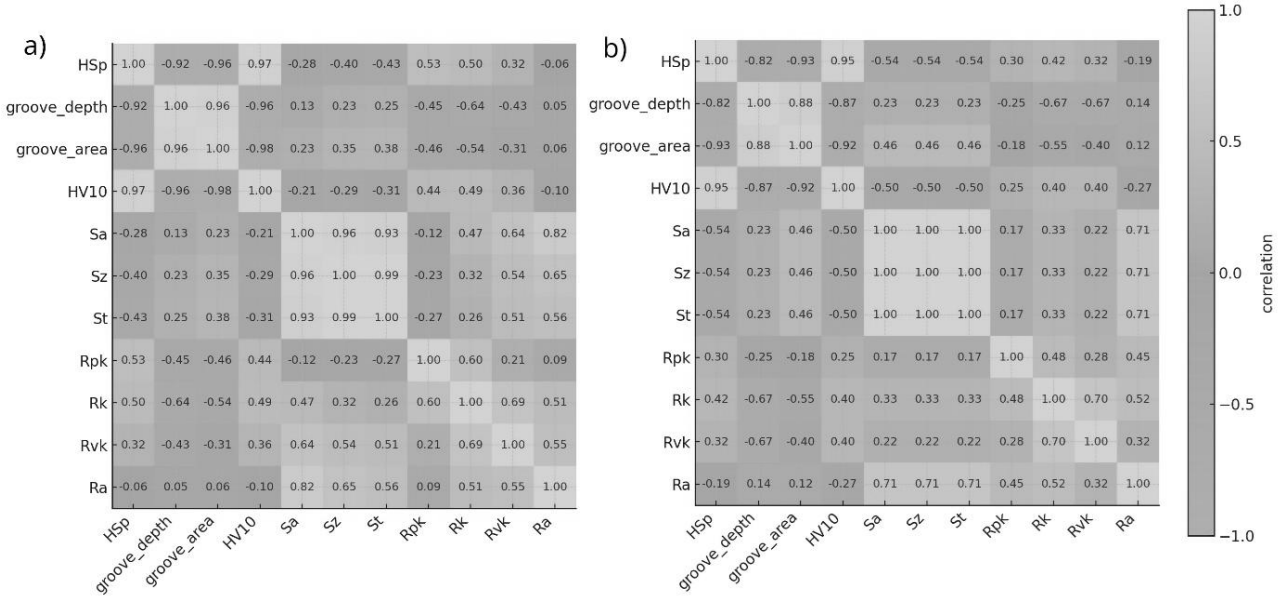

Fig. 7 *Pearson (a) and Spearman (b) correlation matrices between scratch response (HSp. residual groove depth/area). HV10 hardness and texture descriptors (Sa, Sz, St, Rpk, Rk, Rvk, Ra). Cells report correlation coefficients (−1…+1); colour scale: red (negative). blue (near zero). green (positive)*

3.6 Correlation analysis

Figure 7a and 7b present Pearson and Spearman correlation matrices between scratch response (HSp. residual groove depth/area). HV10 hardness and texture descriptors (Sa, Sz, St, Rpk, Rk, Rvk, Ra). Despite the limited sample size (n = 9; three steels × three routes). consistent patterns emerge:

HSp shows a strong positive association with HV10 (Pearson r≈0.97; Spearman ϱ≈0.95). confirming the dominant role of bulk hardness in scratch resistance under the present conditions.

HSp is strongly negative vs. groove depth/area (internal consistency of scratch metrics: higher hardness produces narrower/smaller residual grooves).

Associations with areal extremes are modest and negative (HSp vs. Sz/St). indicating that lower height extremes tend to accompany higher scratch resistance once Ra is matched.

The link to Rpk (peak content) is weak-to-moderate and sign-sensitive across Pearson vs. Spearman. suggesting either nonlinearity or route-specific clusters. best inspected with scatter plots.

HSp vs. Ra is negligible. reinforcing that Ra alone is not a reliable functional predictor in this context.

4 Conclusion

This study assessed how three machining routes. turning. milling. and grinding. affect 3D surface texture and scratch response of three structural steels (C45, 42CrMo4, 30CrMoV9) under conditions where the line-based roughness Ra was deliberately aligned across routes. Areal topography (Talysurf CCI Lite) and bearing-area-curve (BAC) descriptors were evaluated from common 3D maps; scratch resistance was obtained at constant load using a 120° Rockwell indenter. The correlation analysis (Fig. 7) confirms a strong dependence of scratch hardness on bulk hardness and a weak association with Ra. while moderate. route-consistent trends with areal extremes and peak-related metrics underscore the need to specify 3D/BAC descriptors alongside Ra.

Areal metrics outperformed profile Ra in discriminating process signatures. Height extremes Sz

and St re-ranked the routes relative to Ra: turning consistently produced the smallest extremes. milling was intermediate. and grinding exhibited the largest peaks and valleys.

BAC parameters captured functional trade-offs. In the matched-Ra set. turning generally showed the lowest Rpk (reduced peak height) and a stable load-bearing core (Rk); grinding showed the highest Rvk (reduced valley depth). These outcomes are consistent with the observed surface morphologies and indicate differing tendencies for run-in film rupture. load support. and lubricant retention.

Scratch resistance followed material hardness with a secondary process effect. The ranking of HSp across steels mirrored HV10 hardness (C45 < 42CrMo4 < 30CrMoV9). Superimposed on this material trend. turning yielded the highest HSp (narrower residual grooves). milling was intermediate. and grinding the lowest—coherent with the measured areal extremes and peak content.

Tool/wheel condition is a critical covariate. The poorer surface produced by grinding in this dataset is attributable to the recorded wheel state. Comparative studies of machining routes must therefore log and control dressing. balance. and wear. as these factors strongly influence areal extremes and BAC descriptors.

Implications for specification and control. Sole reliance on Ra is inadequate when functional performance matters. For tribological components. specifications should include limits on areal extremes (Sz, St) and BAC parameters (Rpk, Rk, Rvk). together with explicit reporting of process context (e.g. wheel condition). Where run-in stability and damage tolerance are critical. upper bounds on peak-dominated metrics (Rpk, Sz) are advisable; where lubricant retention is beneficial. valley descriptors (Rvk, Svk) should be balanced against extremes.

Limitations and next steps. Replication per variant was limited. and the grinding wheel condition constrained generality. Future work should (i) expand replication to enable formal correlation and uncertainty analysis. (ii) incorporate directionality metrics (e.g.. Str. Sal) to quantify lay effects. and (iii) extend validation to lubricated or rolling contacts to map how the observed texture signatures translate beyond dry. single-pass scratching.

Overall. under matched Ra. turning provided the most favourable combination. advantageous BAC characteristics. and highest scratch resistance in this material set; milling was intermediate; and grinding requires stringent wheel-state control to realise its potential benefits. These findings support adopting 3D areal and BAC descriptors as routine complements to Ra in process qualification and functional surface specification.

Declaration of competing interest

The authors declare that they have no known competing financial interests or personal relationships that could have appeared to influence the work reported in this paper.

Data availability

Data will be made available on request.

Acknowledgement

This research study was supported by the grant "Comprehensive technology for interdisciplinary work with advanced materials emphasizing their multidisciplinary applications". FSI-S-25-8787.

References

[1] PAWLUS, P., REIZER, R., WIECZOROWSKI, M. (2021). Functional importance of surface texture parameters. In: *Materials*, Vol. 14, No. 18, pp. 5326. https://doi.org/10.3390/ma14185326

[2] JIANG, X., WHITEHOUSE, D. J. (2012). Technological shifts in surface metrology. In: *CIRP Annals – Manufacturing Technology*, Vol. 61, No. 2, pp. 815–836. https://doi.org/10.1016/j.cirp.2012.05.009

[3] LEACH, R. K. (2013). *Characterisation of areal surface texture*. Berlin-Heidelberg: Springer. ISBN: 978-3-642-36457-0. https://doi.org/10.1007/978-3-642-36458-7

[4] WHITEHOUSE, D. J. (2010). *Handbook of surface and nanometrology*. 2nd ed. Boca Raton: CRC Press. ISBN: 9780429140693. https://doi.org/10.1201/b10415

[5] GADELMAWLA, E. S., KOURA, M. M., MAKSOUD. T. M. A., ELEWA. I. M., SOLIMAN. H. H. (2002). Roughness parameters. In: *Journal of Materials Processing Technology*, Vol. 123, No. 1, pp. 133–145. https://doi.org/10.1016/S0924-0136(02)00060-2

[6] INTERNATIONAL ORGANIZATION FOR STANDARDIZATION. (2021). ISO 25178-2:2021. Geometrical product specifications (GPS) - *Surface texture: Areal - Part 2: Terms. definitions and surface texture parameters.* Geneva: ISO.

[7] INTERNATIONAL ORGANIZATION FOR STANDARDIZATION. (2021). ISO 21920-2:2021. Geometrical product specifications (GPS) - Surface texture: Profile - Part 2: Terms. definitions and surface texture parameters. Geneva: ISO.

[8] ASTM INTERNATIONAL. ASTM G171-03(2017). (2024). *Standard test method for scratch hardness of materials using a diamond stylus*. West Conshohocken, PA: ASTM International. https://doi.org/10.1520/G0171-03R17

[9] ETSION, I. (2005). State of the Art in Laser Surface Texturing. In: *Journal of Tribology*, Vol. 127, No. 1, pp. 248–253. https://doi.org/10.1115/1.1828070

[10] LEACH, R. K. (2011). *Optical Measurement of Surface Topography*. Berlin-Heidelberg: Springer. ISBN: 978-3-642-12011-4. https://doi.org/10.1007/978-3-642-12012-1

[11] HE, B., ZHENG, H., DING, S., YANG, R., SHI, Z. (2021). A review of digital filtering in evaluation of surface roughness. In: *Metrology and Measurement Systems*, Vol. 28, No. 2, pp. 217–253. https://doi.org/10.24425/mms.2021.136606

[12] FRANCO, L. A., SINATORA, A. (2015). 3D surface parameters (ISO 25178-2): Actual meaning of Spk and its relationship to Vmp. In: *Precision Engineering*, Vol. 40, pp. 106–111. https://doi.org/10.1016/j.precisioneng.2014.10.011

[13] PAWLUS, P., REIZER, R., WIECZOROWSKI, M., KROLZCYK, G. M. (2024). Sensitivities of surface texture parameters to measurement errors - A review. In: *Measurement*, Vol. 227, pp. 114323. https://doi.org/10.1016/j.measurement.2024.114323

[14] SHI, W.-C., ZHENG, J.-M., WANG, G.-L., WANG, Q.-L., LI, Q. (2021). Characterization of machined surface topography based on multi-feature fusion. In: *Micromachines*, Vol. 12, No. 3, pp. 228. https://doi.org/10.3390/mi12030228

[15] PERSSON, B. N. J. (2023). On the Use of Surface Roughness Parameters. In: *Tribology Letters*, Vol. 71, No. 29. https://doi.org/10.1007/s11249-023-01700-z

[16] QI, Q., LI, T., SCOTT, P. J., JIANG. X. (2015). A Correlational Study of Areal Surface Texture Parameters on Some Typical Machined Surfaces. In: *Procedia CIRP*, Vol. 27, pp. 149–154. https://doi.org/10.1016/j.procir.2015.04.058

[17] TODHUNTER, L. D., LEACH, R. K., LAWES, S. D. A., BLATEYRON, F. (2017). Industrial survey of ISO surface texture parameters. In: *CIRP Journal of Manufacturing Science and Technology*, Vol. 19, pp. 84–92. https://doi.org/10.1016/j.cirpj.2017.06.001

[18] ZENG, Q., QIN, Y., CHANG, W., LUO, X. (2018). Correlating and evaluating the functionality-related properties with surface texture parameters and specific characteristics of machined components. In: *International Journal of Mechanical Sciences*, Vol. 149, pp. 62–72. https://doi.org/10.1016/j.ijmecsci.2018.09.044

[19] ABELLAN-NEBOT, J. V., VILA PASTOR, C., SILLER, H. R. (2024). A review of the factors influencing surface roughness in machining and their impact on sustainability. In: *Sustainability*, Vol. 16., No. 5, pp. 1917. https://doi.org/10.3390/su16051917

[20] SINGH, K., PALIWAL, N., KASAMIAS, K. (2024). Surface roughness characterization using a representative elementary area (REA). In: *Scientific Reports*, Vol. 14, No. 1785, pp. 52329. https://doi.org/10.1038/s41598-024-52329-4

[21] COSTA, H. L., HUTCHINGS, I. M. (2014). Some innovative surface texturing techniques for tribological applications. Proceedings of the Institution of Mechanical Engineers. In: *Part J: Journal of Engineering Tribology*, Vol. 229, No. 4., pp. 429–448. https://doi.org/10.1177/1350650114539936

[22] ZHONG, Z. W., VENKATESH, V. C. (2009). Recent developments in grinding of advanced materials. In: *International Journal of Advanced Manufacturing Technology*, Vol. 41, No. 5–6, pp. 468–480. https://doi.org/10.1007/s00170-008-1496-3

[23] CURTIS, D., KRAIN, H., WINDER, A., NOVOVIC. D. (2021). Impact of grinding wheel specification on surface integrity and residual stress when grinding Inconel 718. Proceedings of the Institution of Mechanical Engineers. In: *Part B: Journal of Engineering Manufacture*, Vol. 235, No. 10, pp. 1668–1681. https://doi.org/10.1177/0954405420961209

[24] PAWLUS, P., REIZER, R., WIECZOROWSKI, M. (2020). Characterization of the shape of height distribution of two-process profile. In: *Measurement*, Vol. 153, pp. 107387. https://doi.org/10.1016/j.measurement.2019.107387

[25] SEDLACEK, M., PODGORNIK, B., VIZINTIN, J. (2012). Planning surface texturing for reduced friction using skewness

and kurtosis. Proceedings of the Institution of Mechanical Engineers. In: *Part J: Journal of Engineering Tribology*, Vol. 226, No. 8, pp. 661–667. https://doi.org/10.1177/1350650112439809

[26] SEDLACEK, M., PODGORNIK, B., VIZINTIN, J. (2012). Correlation between standard roughness parameters skewness and kurtosis and tribological behaviour of contact surfaces. In: *Tribology International*, Vol. 48, pp. 102–112. https://doi.org/10.1016/j.triboint.2011.11.008

[27] DINH, T. D. et al. (2021). Modelling detrimental effects of high surface roughness on fatigue: Case of Ti-6Al-4V AM. In: *International Journal of Fatigue*, Vol. 144, pp. 106034. https://doi.org/10.1016/j.ijfatigue.2020.106034

[28] HE, B., PETZING, J., WEBB, P., LEACH, R. (2015). Improving copper plating adhesion on glass using laser machining techniques and areal surface texture parameters. In: *Optics and Lasers in Engineering*, Vol. 75, pp. 39–47. https://doi.org/10.1016/j.optlaseng.2015.06.004

[29] WHITEHOUSE, D. J. (1997). Surface metrology. In: *Measurement Science and Technology*, Vol. 8, No. 9, pp. 955–972. https://doi.org/10.1088/0957-0233/8/9/002

[30] BARTH, S., KLOCKE, F. (2017). Influence of Grinding Wheel Topography on the Thermo-Mechanical Stress Collective in Grinding. In: *Inventions*, Vol. 2, No. 4, pp. 34. https://doi.org/10.3390/inventions2040034

[31] MALY, M., KOLOMY, S., KASAN, R., BARTL, L., SEDLAK, J. et al. (2024). Mechanical Properties, Structure and Machinability of the H13 Tool Steel Produced By Material Extrusion. In: *Manufacturing Technology*, Vol. 24, No. 4, pp. 608–617. ISSN 1213-2489. https://doi.org/10.21062/mft.2024.066

[32] DRBAL, M., KOLOMY, S., SEDLAK, J., ZOUHAR, J., VITEK, J. (2024). Investigation of the Tool Wear Progression in Parting Technology. In: *Manufacturing Technology*, Vol. 24. No. 6, pp. 901–913. ISSN 1213-2489. https://doi.org/10.21062/mft.2024.093

[33] ZEMCIK, O., KOURIL, K., SLANY, M., ZOUHAR, J., SEDLAK, J. et al. (2023). Machinability of UMCo50 Cobalt Superalloy. In: *Manufacturing Technology*, Vol. 23, No. 6, pp. 949–957. ISSN 1213-2489. https://doi.org/10.21062/mft.2023.082

[34] KOLOMY, S., MALY, M., DOUBRAVA, M., SEDLAK, J., ZOUHAR, J. et al. (2025). Effect of microstructure on machinability of extruded and conventional H13 tool steel. In: *Materials & Design*, Vol. 254, pp. 114132. ISSN 0264-1275. https://doi.org/10.1016/j.matdes.2025.114132

[35] KOLOMY, S., SLANY, M., DOUBRAVA, M., SEDLAK, J., ZOUHAR, J. et al. (2025). Comparative analysis of machinability and microstructure in LPBF and conventionally processed M300 maraging steel. In: *Scientific Reports*, Vol. 15, No. 1, pp. 35980-21. ISSN 2045-2322. https://doi.org/10.1038/s41598-025-19719-8